Transactions, SMiRT-22
San Francisco, California, USA - August 18-23, 2013
Division I

HYDROGEN UPTAKE AND ITS EFFECT ON MECHANICAL PROPERTIES OF EUROFER 97-2 AND ODS-EUROFER STEELS

Malitckii E.[1], Yagodzinskyy Y.[1], Ganchenkova M.[1,2], Saukkonen T.[1], Hänninen, H.[1], Lindau R.[3], Vladimirov P.[3], Moeslang A.[3]

[1] Aalto University, School of Engineering, FI-00076 AALTO, Finland
[2]National Research Nuclear University, Moscow, Russian Federation
[3] Karlsruhe Institute of Technology, Institute for Applied Materials, Germany

ABSTRACT

Hydrogen effects on the mechanical tensile properties of the ferrite-martensite EUROFER 97-2 and ODS-EUROFER steels were studied at room temperature. Hydrogen was introduced into the steels with electrochemical charging method from 0.1N NaOH solution under controlled potential. Hydrogen uptake and its trapping energy are calculated from the thermal desorption spectra obtained for the studied steels in the temperature range from room temperature to 1123 K. It was found that hydrogen concentration in ODS-EUROFER is markedly higher than in EUROFER 97-2 steel due to its trapping at interfaces between steel matrix and yttria nanoparticles.

In the case of hydrogen charging at low electrochemical potential of -1.7 $V_{Hg/Hg2SO4}$, hydrogen has only a minor effect on the mechanical properties of studied materials. With increase of hydrogen charging at -1.85 $V_{Hg/Hg2SO4}$ both steels manifest significant sensitivity to hydrogen embrittlement. Hydrogen results in reduction of elongation to fracture with just a slight effect on the yield stress, but fracture surface morphology manifests rather different structures such as: areas of intergranular fracture in ODS steel and ductile dimpled fracture in EUROFER 97-2. The mean particle size, chemical composition and microstructural changes induced by hydrogen are revealed with TEM and SEM observations. The hydrogen embrittlement in the form of intergranular fracture of ODS-EUROFER steel was observed by FEG-SEM fractography, and the role of yttria nanoparticles in the intergranular fracture formation is discussed.

INTRODUCTION

With the development of Generation IV nuclear reactors and the accelerator-driven systems (ADS) for nuclear waste incineration the requirements for the structural materials have increased substantially. The advanced energy generation facilities are intended to operate at temperatures (from 500 to 1000 °C) well above the limit of microstructural stability of the used ferrite-martensite steels. The maximum fluence for core internal structures of Gen IV nuclear reactors is much higher (from 30 to 150 dpa) than it was in previous generation of reactors. Both helium and hydrogen accumulated in the steel due to the (n,α) and (n,p) transmutation reactions lead to swelling effect and radiation-induced property degradation. The present structural materials are sensitive to the above-mentioned deleterious effects which may operate in a synergistic way.

It is assumed, that strengthening of the steel with nano-sized particles of yttrium or mixed (Y-Al/Ti) oxides is a promising way to improve resistance to radiation damage under height neutron fluence levels. At the same time, the strengthening results in enhanced thermal and radiation creep ductility at temperatures up to 600 °C, Schäublin (2006), Lindau (2002). However, with increasing neutron fluence in reactor or ADS devices helium and hydrogen produced by nuclear transmutations can cause gas-induced embrittlement or swelling and it is not obvious how the presence of dispersion-strengthening nanoparticles affects the gas-induced property changes. It is expected that fine oxide particles can effectively trap the gas atoms on their interfaces, which appear as shells surrounding the amorphous layer

of nanoparticles, Hsiung (2010). The trapping on the strengthening particle interfaces prevents the vacancy and mutual gas precipitation at the carbide particle interfaces and grain boundaries resulting in the reduction of gas swelling, Hsiung (2010), Kompaniets (2009). Even though the mechanism of helium bubble formation at the manufacturing stages or under irradiation of the ODS steels is discussed, the hydrogen effects have not been studied in detail, yet.

Another effect of the hydrogen accumulation in the ODS steels is the hydrogen embrittlement, which may appear at ambient temperatures after cooling down the steel components of a nuclear power plant from the high operation temperatures. The hydrogen trapping at the yttria nanoparticle interfaces in the ODS steels can affect their sensitivity to hydrogen embrittlement in comparison to that in the case of ferritic or ferrite-martensite Cr-alloyed steels.

The aim of the present work consists of a comparative study of hydrogen uptake in EUROFER 97-2 and ODS-EUROFER steels and their sensitivity to hydrogen embrittlement. A special attention is paid to the role of dispersion-strengthening yttria nanoparticles in the possible mechanism of hydrogen embrittlement of ODS steels.

EXPERIMENTAL

Oxide-dispersion strengthened ferrite-martensite ODS-EUROFER and EUROFER 97-2 steels were chosen for the study. As shown in Table 1, both steels have almost the same chemical composition except for the addition of 0.3 wt.% Y_2O_3 in ODS-EUROFER steel. Such a choice of materials allows to estimate the influence of yttria nanoparticles on hydrogen trapping and mechanical properties.

Table 1: Chemical composition of ODS-EUROFER and EUROFER 97-2 steels in wt.%.

Sample	C	Si	Mn	Cr	Ni	Mo	Al	W	V	Ti	Co
ODS-EUROFER	0.086	0.03	0.39	9.2	0.02	0.0056	0.003	1.14	0.1965	<0.003	0.0036
EUROFER 97	0.11	0.03	0.55	8.95	0.013	<0.005	0.009	1.06	0.202	<0.003	0.004

Billets of the CERT specimens were cut from block of each material with a spark erosion machine. The sub-sized tensile test specimens were cut longitudinally to the rolling direction with a gauge length of 0.2 × 4 × 9 mm. Another set of the plate specimens with size 0.2 × 4 × 7 mm was prepared for TDS measurement of hydrogen uptake and trapping in the studied steels. Samples were mechanically polished finishing with 3 μm diamond paste.

Hydrogen charging was performed electrochemically in 0.1N NaOH solution with 20 mg/l of $CS(NH_2)_2$ at controlled potential and temperature of 300 K in a cell. The cell consists of a double-wall glass compartment with Luggin-probe of Hg/Hg_2SO_4 reference and Pt counter electrodes. The electrolyte for hydrogen charging was pumped and circulated between the cell and an additional compartment used for the solution de-aeration.

Hydrogen charging was performed at -1.7 $V_{Hg/Hg2SO4}$ and -1.85 $V_{Hg/Hg2SO4}$ applied electrochemical potentials in order to estimate the hydrogen concentration effect on the mechanical properties of the materials. Since the coefficient of hydrogen diffusion in EUROFER 97-2 and ODS-EUROFER steels is found to be $D(T) = 4.57 \times 10^{-7} exp(-22300/RT)$ and $D(T) = 1.33 \times 10^{-6} exp(-30400/RT)$ m^2/s, Esteban (2007), the suitable hydrogen charging time was estimated to provide the homogeneous hydrogen distribution over the sample cross-section.

Hydrogen uptake and trapping were measured with TDS method in the temperature range from room temperature to 1123 K. Hydrogen desorption flux was measured with mass-spectrometer in ultra-high vacuum (UHV) chamber with basic vacuum better than 10^{-8} mbar. Parameters of hydrogen trapping were obtained using activation analysis, Choo (1982), Kissinger (1957), with heating rate varied from 2 to 8 K/min, while the hydrogen uptake in tensile test samples was measured at heating rate of 6 K/min.

Tensile CERT tests were carried out using a 2 kN DEBEN load cell equipped with an optical strain monitoring system. Microstructure characterization and fractography of the steels were performed with TEM Zeiss LIBRA 120 and FEG SEM Zeiss 55 Ultra.

RESULTS AND DISCUSSION

Typical TEM micrographs of ferrite-martensite EUROFER 97-2 and ODS-EUROFER steels are shown in Figure 1. Both materials manifest grains elongated along the rolling direction with a smallest size of about 1 μm. A number of Cr and W carbide particles located preferably at grain boundaries are visible on micrographs of both steels, while ODS-EUROFER steel manifests additionally yttria nanoparticles homogeneously distributed in every grain as shown in the insert of Figure 1. Carbide particle size is about 200 nm for both steels. The density of yttria nanoparticles in ODS steel was estimated to be about $1 \cdot 10^{22}$ m^{-3} with average particle size of about 25 nm.

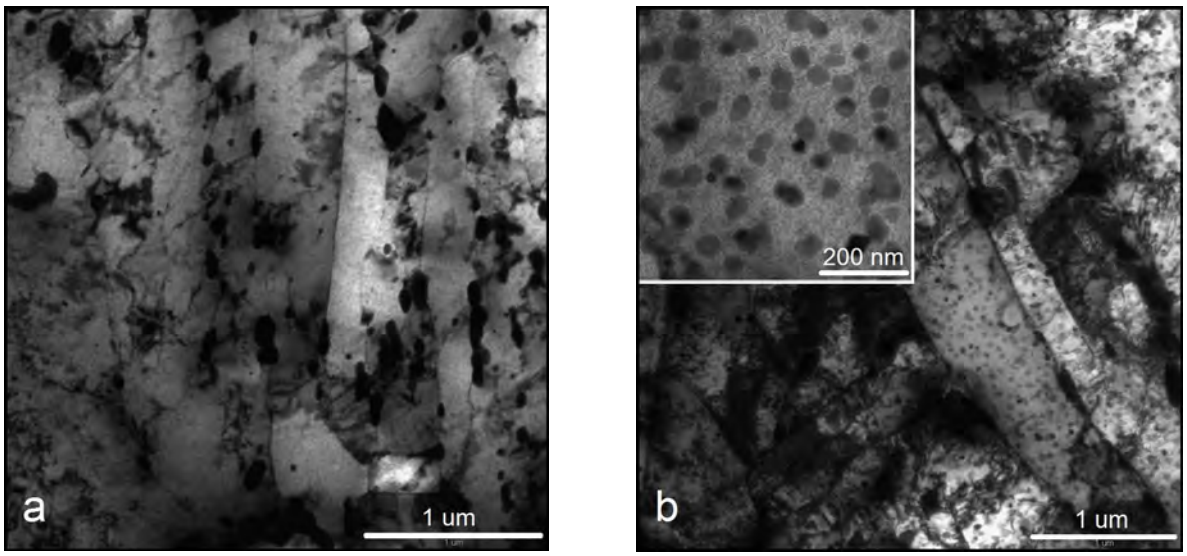

Figure 1. TEM micrographs of EUROFER 97-2 (a), and ODS-EUROFER (b) steels. Insert shows a high magnification of ODS-EUROFER steel micrograph with yttria nanoparticles.

Hydrogen uptake of the steels was evaluated by comparison of the TDS peaks of the hydrogen-free and hydrogen-charged specimens. The TDS curves of the studied steels manifest a single peak with maximum desorption rate temperature at about 415 and 405 K for ODS-EUROFER and EUROFER 97-2 steels at the heating rate of 6 K/min, respectively (see Figure 2). Concentrations of accumulated hydrogen are defined by the area under the obtained TDS curves. Total concentration of hydrogen in ODS-EUROFER steel is found to be 29 at. ppm. If the specimen is kept at room temperature for 24 h the hydrogen concentration decreases to 22.5 at. ppm. On the other hand, EUROFER 97-2 steel charged at the same condition uptakes only about 7 at. ppm of hydrogen. One can conclude that yttria nanoparticles in ODS-EUROFER steel are considerable trapping sites for hydrogen.

Activation analysis of the obtained TDS peaks was performed for heating rates in the range from 2 to 8 K/min using the procedure proposed by Choo and Lee (1982). Activation energies E_a of hydrogen de-trapping were obtained using Equation 1, Kissinger (1957):

$$\frac{d\left[\ln\left(\frac{dT/dt}{T_m^2}\right)\right]}{d\left[\frac{1}{T_m}\right]} = -\frac{E_a}{k_B} \qquad (1)$$

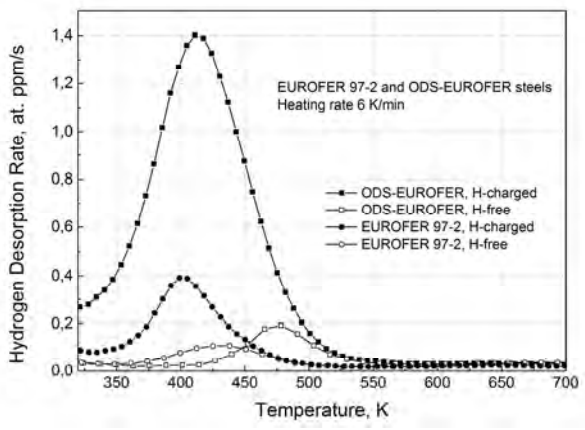

Figure 2. TDS spectra for hydrogen release from H-free and H-charged (at -1.7 $V_{Hg/Hg2SO4}$) EUROFER 97-2 and ODS-EUROFER steels. Heating rate is 6 K/min.

where dT/dt is the heating rate, T_m is the temperature of the peak maximum, and k_B is the Boltzmann`s constant. Thereby, using the linear regression slope of $\ln[(dT/dt)/T_m^2]$ *vs* $1/T_m$ shown in Figure 3 a the effective activation energy for release of hydrogen atoms from the trapping sites is calculated. The analysis was applied for both studied materials. The effective activation energies of hydrogen trapping is found to be about 0.33 eV for ODS-EUROFER steel that is rather different than 0.23 eV obtained for EUROFER 97-2 steel. The obtained results evidence that yttria nanoparticles in ODS-EUROFER steel operate as effective trapping sites for hydrogen. The results correspond well with data obtained by the gas permeation technique for EUROFER 97 steel (E_d = 0.23 eV) and ODS-EUROFER steel (E_d = 0.32 eV), Esteban (2007).

In order to clarify the hydrogen trapping nature in ODS-EUROFER steel the activation analysis was repeated for ODS steel samples kept at room temperature for 24 h after hydrogen charging at electrochemical potential of -1.7 $V_{Hg/Hg2SO4}$. Figure 3 b show the TDS curves for different desorption rates from 2 to 8 K/min of hydrogen-charged ODS-EUROFER steel after dwell time of 24 h.

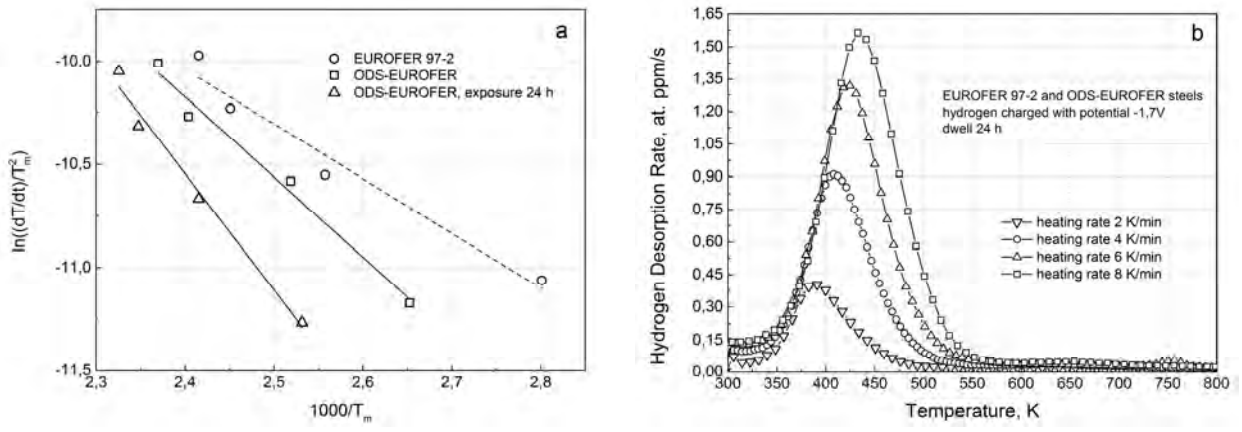

Figure 3. Dependence of $\ln((dT/dt)/T_m^2)$ on $1/T_m$ for EUROFER 97-2 and ODS-EUROFER (a), TDS spectra for different heating rates from 2 to 8 K/min after dwell time of 24 h for ODS-EUROFER steel after hydrogen charging at -1.7 $V_{Hg/Hg2SO4}$ (b).

The hydrogen concentration is found to be about 22.5 at.ppm that is slightly less than obtained for ODS steel samples without dwelling. Also, it should be noted, that dwelling in air for 24 h shifts the temperature maximum of TDS curves to higher temperatures (see Figure 4) and it results in an increase of the effective activation energy of hydrogen de-trapping from 0.33 to 0.48 eV.

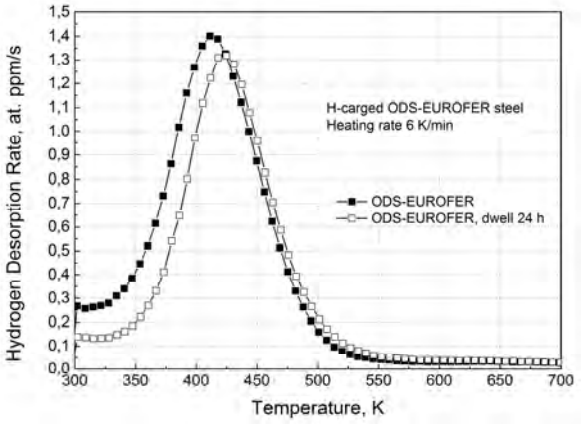

Figure 4. TDS spectra of hydrogen pre-charged ODS-EUROFER steel after charging and 24 dwell time. Heating rate 6 K/min.

The last result evidences that hydrogen trapping energy at the interfaces of yttria nanoparticles has a broad distribution. In other words, at low hydrogen concentration hydrogen occupies energetically deeper trapping sites at the interfaces. With increase of hydrogen concentration the hydrogen trapping sites are successively occupied. This dependence indicates that the binding energy of trapped hydrogen cannot be obtained as a single value, but it consists of a range of energy states at the yttria nanoparticle interfaces. The summarized results of the obtained activation energies are shown in Table 2.

Table 2: Activation energies of hydrogen obtained from activation analyses of TDS peaks of EUROFER 97-2 and ODS-EUROFER steels.

Material	Energy (eV)
EUROFER 97-2	0.23 ± 0.03
ODS-EUROFER	0.33 ± 0.03
ODS-EUROFER (dwell 24 h)	0.48 ± 0.04

The CERT results of EUROFER 97-2 and ODS-EUROFER steels are shown in Figures 5 a and b. Samples of both studied materials were pre-charged electrochemically at room temperature at applied potentials of -1.7 $V_{Hg/Hg2SO4}$ and -1.85 $V_{Hg/Hg2SO4}$. In as-supplied condition the ODS-EUROFER steel manifests tensile strength of about 1100 MPa which is markedly higher than that of EUROFER 97-2 steel (690 MPa). The elongation to fracture of ODS-EUROFER steel is about 8 %, which is markedly less than that for EUROFER 97-2 steel, 13 %.

Hydrogen-charging at potential -1.7 $V_{Hg/Hg2SO4}$ results only in a minor effect on the tensile properties of both studied steels. However, the results change dramatically when the applied hydrogen charging potential decreases to -1.85 $V_{Hg/Hg2SO4}$. The elongation to fracture of EUROFER 97-2 steel reduces to 8 %. At the same time, no change of tensile strength was observed as seen in Figure 5 b. ODS-EUROFER steel charged at the same electrochemical potential manifests elongation to fracture of about 4 % (see Figure 5 a).

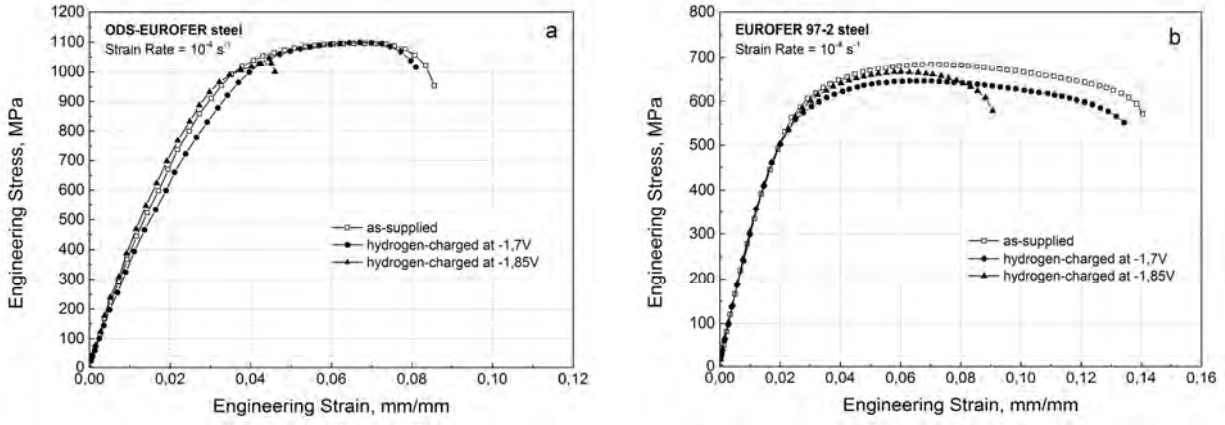

Figure 5. CERT stress-strain curves of ODS-EUROFER steel (a) and EUROFER 97-2 steel (b) in as-supplied state (open symbols) and after electrochemical hydrogen charging at -1.7 $V_{Hg/Hg2SO4}$ and -1.85 $V_{Hg/Hg2SO4}$ (filled symbols). Strain rate 10^{-4} s^{-1}.

Fractography of EUROFER 97-2 and ODS-EUROFER steels after tensile test in as-supplied state is shown in Figure 6 a and b, respectively. Without hydrogen both steels manifest a typical ductile dimpled fracture surface with Cr and W carbide particles observed often in the dimples. Hydrogen charging with electrochemical potential of -1.7 $V_{Hg/Hg2SO4}$ does not change dramatically the CERT fracture modes of EUROFER 97-2 and ODS-EUROFER steels. In this case, on the fracture surface of EUROFER 97-2 steel a net of short secondary cracks appears as shown in Figure 6 c. The cracks have a typical length of a few tens of micrometers with preferable orientation parallel to the rolling direction. Observation with high magnification evidences that short randomly oriented secondary cracks (see insert in Figure 6 c) form in EUROFER 97-2 steel. ODS-EUROFER steel manifests rather similar fracture features in CERT after hydrogen charging at -1.7 $V_{Hg/Hg2SO4}$. In this case, however, no elongated secondary cracks were observed, while the randomly distributed short cracks are present on fractographs as shown in Figure 6 d. ODS-EUROFER steel reveals often the carbide particles as shown in the insert of Figure 6 d.

Hydrogen charging of the studied steels at high fugacity (-1.85 $V_{Hg/Hg2SO4}$) results in dramatic changes of the fracture mode of ODS-EUROFER steel. At the same time, fractography of EUROFER 97-2 steel evidences changes of ductile dimpled fracture. In the last case, however, some dimples look like hydrogen-induced voids as shown in the insert of Figure 6 e. Hydrogen charging at potential of -1.85 $V_{Hg/Hg2SO4}$ of ODS-EUROFER steel results in clear hydrogen embrittlement in the form of “fish eye” as shown in Figure 6 f.

In addition to “fish eyes” another hydrogen embrittlement mode was observed in this case, namely, intergranular hydrogen-induced fracture at the corners of the specimens as shown in Figure 7 a and b. Brittle areas of the “fish eye” consist of brittle facets with characteristic length comparable with grain size of the steel evidencing also on the intergranular fracture mode induced by hydrogen of high fugacity. Detailed view of the brittle fracture facets shown in Figure 7 b reveals a numbers of yttria nanoparticles (white dots) and dimples from exfoliated nanoparticles.

One can assume that in the presence of hydrogen the yttria nanoparticles at the grain boundaries may decrease the grain boundary cohesion resulting in intergranular fracture of the ODS-EUROFER steel. It seems that intergranular fracture of the steel takes place when hydrogen concentration exceeds a certain critical value. The similar effect of hydrogen was already observed, Lee (2004), where the threshold character of hydrogen embrittlement after electrochemical hydrogen charging was observed in tensile tested ferrite-martensite 9Cr – 2W steel and K-type ferrite ODS steels. If the external stress induces additional trapping sites at grain boundaries, the stress application may result in the re-distribution of hydrogen between matrix particle interfaces and grain boundaries. The higher the hydrogen trapping ability of the steel is, the more hydrogen is provided at the grain boundaries. The

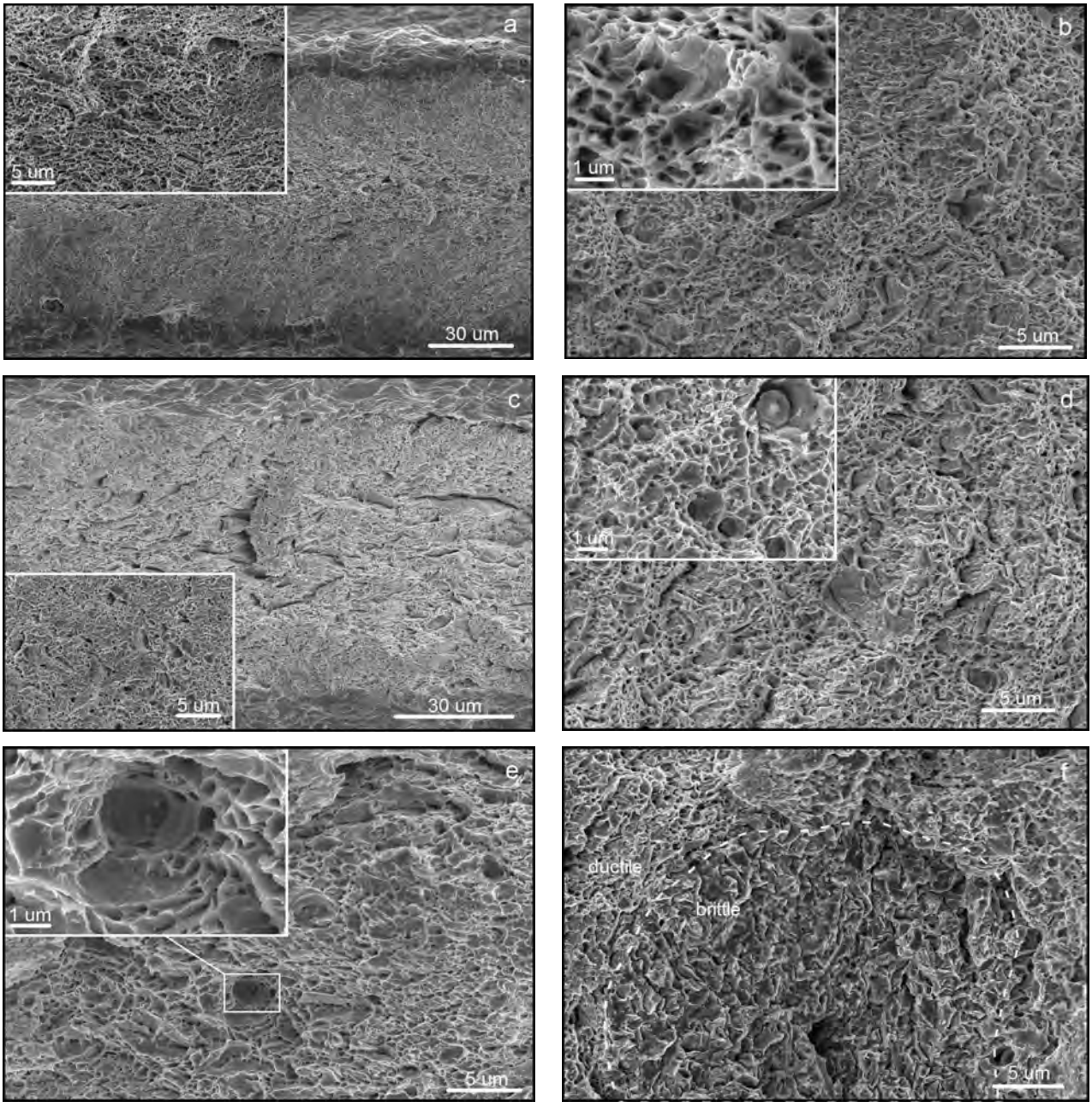

Figure 6. Microstructures of the fracture surface of EUROFER 97-2 tested as-supplied (a), hydrogen pre-charged at -1.7 $V_{Hg/Hg2SO4}$ (c) and -1.85 $V_{Hg/Hg2SO4}$ (e), and ODS-EUROFER tested as-supplied (b), hydrogen pre-charged at -1.7 $V_{Hg/Hg2SO4}$ (d) and -1.85 $V_{Hg/Hg2SO4}$ (f).

threshold character of the hydrogen-induced intergranular fracture of ODS-EUROFER steel may be explained, if the grain boundary de-cohesion takes place, at a certain critical hydrogen concentration. EUROFER 97-2 steel also shows a reduction of elongation to fracture at a higher hydrogen concentration. Probably the same mechanism of hydrogen re-distribution takes place in EUROFER 97-2 steel. However, in this case, the hydrogen concentration of the steel is not enough to provide the critical hydrogen concentration for de-cohesion of grain boundaries. It seems that hydrogen-induced fracture of EUROFER

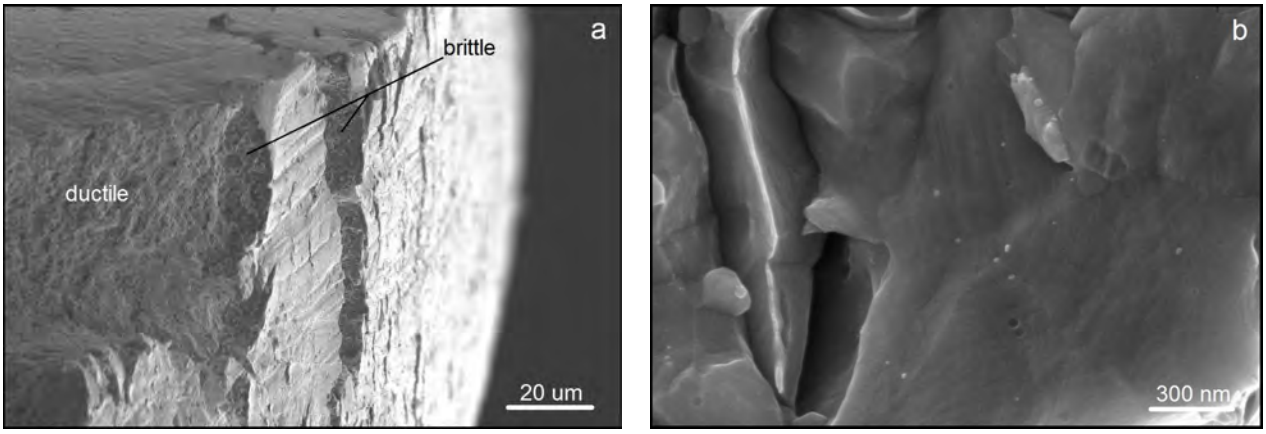

Figure 7. Brittle crack initiation sites at the specimen corners (a) and detail of fracture surface (b) obtained after tensile test of hydrogen pre-charged ODS-EUROFER steel (-1.85 $V_{Hg/Hg2SO4}$).

97-2 steel initiates at the carbide particles by hydrogen-filled voids nucleating at the particle/matrix interfaces. The density of the voids depends probably on the hydrogen fugacity. More detailed mechanism of the hydrogen-induced fracture of the studied steels needs, however, a further comprehensive study.

CONCLUSIONS

Hydrogen uptake and its effect on mechanical properties were studied for EUROFER 97-2 and ODS-EUROFER steels. Hydrogen absorption in ODS steel is markedly higher than it is in EUROFER 97-2 due to hydrogen trapping at the interfaces between yttria nanoparticles and steel matrix. Hydrogen concentration in ODS-EUROFER steel is a few times higher than that in EUROFER 97-2 steel after electrochemical hydrogen charging with the same charging conditions. Effective activation energy of hydrogen trapping is markedly higher for ODS-EUROFER steel than for EUROFER 97-2 steel.

After hydrogen charging at -1.7 $V_{Hg/Hg2SO4}$, hydrogen has only a minor effect on the mechanical properties of the studied materials. With increase of hydrogen concentration (after hydrogen charging at -1.85 $V_{Hg/Hg2SO4}$) ODS-EUROFER and EUROFER 97-2 steels manifest rather different sensitivity to hydrogen embrittlement. Hydrogen results in reduction of elongation to fracture with a slight effect on the yield stress, but fracture surface morphology manifests rather different structures such as intergranular fracture areas in ODS-EUROFER steel and ductile dimpled fracture in EUROFER 97-2. One can conclude that yttria nanoparticles increase the hydrogen uptake and cause intergranular brittle fracture of ODS-EUROFER steel due to the reduction of grain boundary cohesion by re-distribution of hydrogen from yttria nanoparticle interfaces to grain boundary traps. Hydrogen-induced fracture of EUROFER 97-2 steel initiates at the carbide particles by hydrogen-filled voids nucleating at the particle/matrix interfaces.

ACKNOWLEDGEMENTS

The research was supported in part by the Academy of Finland, Doctoral Programme for Nuclear Engineering and Radiochemistry (YTERA, Finland), and by the Federal Target Program contract # 14.740.11.1130 from the Russian Ministry of Education and Science.

REFERENCES

Choo W.Y., Lee J.Y. (1982). ”Thermal analysis of trapped hydrogen in pure iron”, *Metallurgical Transactions* A 13, 135.

Esteban G.A., Peña A., Legarda F., Lindau R. (2007). ”Hydrogen transport and trapping in ODS-EUROFER”, *Fusion Engineering and Design* 82, 2634-2640.

Kissinger H.E. (1957). ”Reaction kinetics in differential thermal analysis”, *Analytical Chemistry* 29, 1702.

Kompaniets T.N. (2009). ”Problem of steel selection for DEMO fusion reactor”, *VANT. Fusion Series* 3, 16-24.

Lee J.S., Kimura A., Ukai S., Fujiwara M. (2004). ”Effects of hydrogen on the mechanical properties of oxide dispersion strengthening steels”, *Journal of Nuclear Materials* 329-333, 1122-1126.

Lindau R., Möslang A., Schirra M., Schlossmacher P., Klimenkov M. (2002). ”Mechanical and microstructural properties of a hipped RAFM ODS-steel”, *Journal of Nuclear Materials* 307-311, 769-772.

Hsiung L.L., Fluss M.J., Tumey S.J., Choi W.B., Serruys Y., Willaime F., Kimura A. (2010). ”Formation mechanism and role of nanoparticles in Fe-Cr ODS steels developed for radiation tolerance”, *Physical Review* B 82, 184103.

Schäublin R., Ramar A., Baluc N., de Castro V., Monge M.A., Leguey T., Schmid N., Bonjour C. (2006). ”Microstructural development under irradiation in European ODS ferritic/martensitic steels”, *Journal of Nuclear Materials* 351, 247-260.